Nationaal Lucht- en Ruimtevaartlaboratorium
National Aerospace Laboratory NLR

NLR-TP-2001-204

CR*spray* - Impingement drag calculation of aircraft on water-contaminated runways

J.H.M. Gooden

DOCUMENT CONTROL SHEET

	ORIGINATOR'S REF.		SECURITY CLASS.
	NLR-TP-2001-204		Unclassified

ORGINATOR
National Aerospace Laboratory NLR, Amsterdam, The Netherlands

TITLE
CR*spray* - Impingement drag calculation of aircraft on water-contaminated runways

PRESENTED AT:
The 48th CASI Annual Conference, Toronto, April 29 - May 2, 2001

AUTHORS	DATE	pp	ref
J.H.M. Gooden	October 2001	15	13

ABSTRACT
This paper describes an engineering method developed for calculating the water spray and the precipitation drag for aircraft on water-contaminated runways. The spray is considered to consist of a large number of individual particle trajectories. A Monte Carlo approach is followed to obtain realistic spray characteristics. Precipitation drag is calculated from the impingement of this spray on the aircraft. Empirical constants were being determined using data from available experiments and flight test results. The calculated precipitation drag compares well with the available flight test data. Results are described among which the contribution of bow spray, the effects of lift variation, geometry variation, tyre pressure and pool height variation.

Nationaal Lucht- en Ruimtevaartlaboratorium
National Aerospace Laboratory NLR

NLR-TP-2001-204

CR*spray* - Impingement drag calculation of aircraft on water-contaminated runways

J.H.M. Gooden

This investigation has been carried out under a contract awarded by European Commission (project CONTAMRUNWAY), contract number AI-96-SC-170, and partly as a part of NLR's basic research programme, Work Plan number L.1.C.4.
European Commission has granted NLR permission to publish this report.

This report is based on a presentation held at the 48th CASI Annual Conference, Toronto, April 29 – May 2, 2001.

Division:	Fluid Dynamics
Issued:	October 2001
Classification of title:	Unclassified

Symbols

AF	atomisation fraction [-]
B_F	effective local impingement width [m]
C_L	aircraft lift coefficient [-]
c	local wing chord [m]
c_f	local shear coefficient [-]
D_C	drag-component of the collision force [N]
D_S	surface shear drag contribution [N]
d_P	diameter of impinging particle [m]
d_R	diameter of reflected particle [m]
e	particle collision restitution coefficient [-]
$\breve{F}_C$	collision force vector [N]
G	velocity inside surface water film [m]
G_F	magnitude of velocity vector $\breve{G}_F$ [m/s]
$\breve{G}_F$	surface water film edge velocity vector [m/s]
$\breve{G}_N$	component of velocity vector $\breve{G}_P$ normal to the aircraft surface [m/s]
$\breve{G}_P$	velocity vector of impinging particle [m/s]
$\breve{G}_R$	velocity vector of reflected particle [m/s]
$\breve{G}_T$	component of velocity vector $\breve{G}_P$ tangential to the aircraft surface [m/s]
$\dot{m}_F$	particle mass flow added to water film [m^3/s]
$\dot{m}_P$	impinging particle mass flow [m^3/s]
$\dot{m}_R$	reflected particle mass flow [m^3/s]
n	ordinate in direction normal to the surface
$\breve{n}$	normal vector to the aircraft surface
p_i	tyre inflation pressure [bar]
U_F	component of $\breve{G}_F$ in along aircraft longitudinal axis [m/s]
U_P	component of $\breve{G}_P$ in along aircraft longitudinal axis [m/s]
U_R	component of $\breve{G}_R$ in along aircraft longitudinal axis [m/s]
V	aircraft rolling speed [m/s]
V_F	local, accumulated water film volume flow [m^3/s]
V_p	maximum drag speed (also termed: hydroplaning reference speed) [m/s]
X_A	aircraft longitudinal axis [m]
δ	boundary layer thickness [m]
δ^*	boundary layer displacement thickness [m]
ρ	water film density [kg/m^3]
$\breve{\tau}$	local shear force exerted by water film on aircraft surface [Pa]
θ	boundary layer momentum loss thickness [m]

Contents

(15 pages in total)

CR*spray* - Impingement drag calculation of aircraft on water-contaminated runways

J.H.M. Gooden
National Aerospace Laboratory NLR,
P.O. box 153, Emmeloord
The Netherlands
tel. +31 527 24 8669
gooden@nlr.nl

Abstract

This paper describes an engineering method developed for calculating the water spray and the precipitation drag for aircraft on water-contaminated runways. The spray is considered to consist of a large number of individual particle trajectories. A Monte Carlo approach is followed to obtain realistic spray characteristics. Precipitation drag is calculated from the impingement of this spray on the aircraft. Empirical constants were being determined using data from available experiments and flight test results. The calculated precipitation drag compares well with the available flight test data. Results are described among which the contribution of bow spray, the effects of lift variation, geometry variation, tyre pressure and pool height variation.

1 Introduction

An aircraft rolling on a runway contaminated by standing water experiences an increased drag force known as precipitation drag. The airworthiness regulations (AMJ 25X1591) give a simple expression to estimate the precipitation drag. This empirical relation is based on the results of pool tests performed in the 60's on transport aircraft (Convair 880, Trident). This approach is much too simple to give a reasonably accurate estimate of the precipitation drag, especially for aircraft of size different from those on which the expression is based. This urged the development of a method for determining the precipitation drag of aircraft in a better way. Within the framework of the Brite-Euram project 'CONTAMRUNWAY', NLR developed a semi-empirical engineering method, called 'CR*spray*' ('Contaminated Runway Spray') which gives promising results. As a byproduct engine ingestion flow rates can be calculated.

The heart of the spray-calculation presented here is a water-droplet trajectory calculation. In order to start the trajectory calculation initial values of particle properties as velocity vector and particle diameter at the spray front are required. Presently, the initial properties are given as a set of purely empirical equations derived from available experimental data. These empirical relations can be improved if more knowledge becomes available on the complex physical processes that take place inside the water pool at the surface wave front.

Disturbances in the flow field, e.g. caused by the presence of the wing or wind are taken into account in an approximate way. The same is done for the airflow generated by the spray itself as a result of entrainment. This paper describes

the way the spray is modeled and the results obtained.

Given the spray properties, the precipitation drag of an aircraft can be calculated. This drag consists of two main components, usually called displacement drag and impingement drag. The first is a result of the work performed by the tyres breaking their way through the water pool and clearing the water from the track. This drag is calculated using a ESDU method which is slightly modified. The impingement drag consists of two parts: collision drag and shear drag. This paper describes the theoretical background and results of the impingement drag calculation. Flight test results for the Cessna Citation II, the Dassault Falcon 2000 and the SAAB 2000 were used to develop the method. Results for the Citation are shown in this paper.

2 Spray pattern calculation

A tyre rolling through a water pool develops a wave front because the water, standing on the runway, is washed away from the tyre track. If this happens with sufficient speed, the resulting wave contains so much energy that the water surface tension force can no longer keep the wave integrated and particles start to separate into a spray. If the phase-speed of the sideways moving spray front wave is constant, a straight wave front will develop. This is what indeed generally can be inferred from pictures of spray tests. In front of the tyres a bow shaped wave front develops, ejecting a spray in forward and upward direction. For side-by-side tyres the sideways wave fronts in between the tyres merge into a single straight centre-wave front along the symmetry plane between the tyres.

Although this is a simplification of reality, the present method considers the full spray to be composed of a large number of individual particle trajectories originating at the described surface wave front and having no mutual interaction. Modeling of the initial conditions for these trajectories is done using empirical relations. For this purpose the rudimentary ESDU spray description (ESDU 83042, 1998) is used as a starting line. The ESDU method gives the location of the most intense part of the side and centre sprays in the shape of a simple trapezoidal bounded area (fig 1).

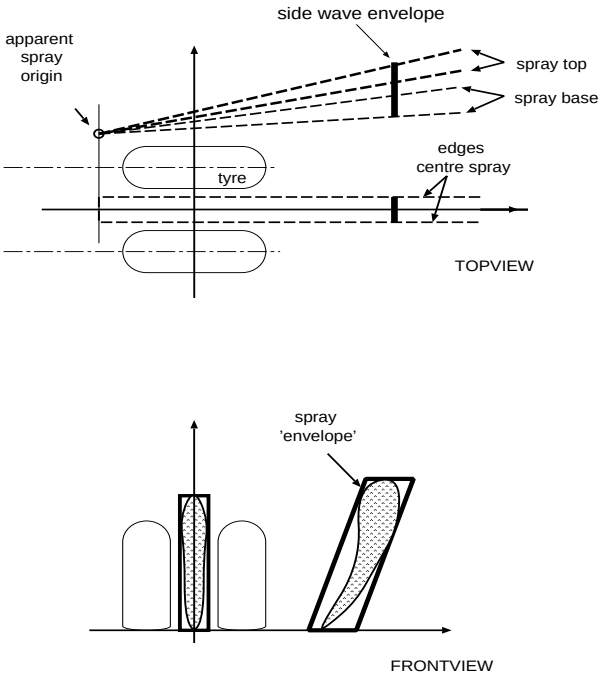

Figure 1: ESDU spray description

The ESDU description is too concise to derive all the initial quantities and, moreover, it does not contain the bow spray in front of the undercarriage. Nevertheless, it offers the big advantage that spray-data of a relatively large number of different undercarriage and tyre combinations have been considered to develop the model. Another limitation of the ESDU model is that it assumes a linear vertical spray development, which only holds for the initial part of the spray close to the tyres. For the development of the present model this constitutes no limitation as the ESDU data are only used for the generation of some of the initial conditions (wave-front location, initial velocity vector and the variance in the latter). Other required initial conditions (spray density, bow wave properties) are modeled using spray-data obtained at NASA by Daugherty & Stubbs

(1987) and tests performed at Bristol University by Barrett (1963, 1965). Besides, data obtained from flight tests with the NLR Citation (Giesberts, 1997), the SAAB 2000 and the Dassault Falcon 2000 have been used to model the spray and spray reflection on the aircraft.

Gaussian variation on a number of relevant initial conditions is applied, leading to a Monte-Carlo type of approach. The initial conditions, to which Gaussian variation was applied, were chosen depending mainly on the sensitivity of the spray shape and the final impingement drag results on these variations.

2.1 Spray main initial parameters

This paper does not allow describing the derivation of all initial parameters extensively. Therefore a short survey of the parameters used is given here. The model includes a number of empirical parameters adapted to give a good comparison between calculation and measured data. The initial conditions modeled are:

Hydroplaning reference speed: related to the AMJ maximum drag speed V_p by an empirical factor. For water, AMJ gives:

$$V_p = 17.6\sqrt{p_i}$$

(p_i tyre inflation pressure in bar, V_p in m/s)

Bow and side wave front location: the ESDU-envelope is tuned to the most intense, upper part of the spray. Nevertheless, the sideways position of the *surface* wave front has been related to the ESDU-data, for reasons of consistency, and is taken as a fraction of the sideways position of the inner edge of the base of the ESDU-spray (figure 1). The (straight) side wave front in CR*spray* is assumed not to start at the hypothetical origin, originally defined by ESDU, but slightly further downstream, in order to accommodate for the bow wave front. The bow-wave front is taken elliptically shaped, split up at the apex by a straight centre part in case of side by side tyres.

Particle initial velocity vector: estimated from the shape and downstream expansion of the ESDU envelope. The particles are released normal to the wave front. It is furthermore assumed that there is an exponential decay of the initial velocity with distance downstream along the wave front. The bow-wave initial spray velocity is taken proportional to the hydroplaning speed V_p. Close to and above hydroplaning the bow-wave disappears as is observed in experiments. Therefore, the elevation angle at the bow-wave apex is taken as a function of aircraft velocity V relative to V_p using experimental data given by Maltby & Slatter (1969) and the flight test results. Maltby & Slatter report that the bow-wave elevation angle depends on the aircraft velocity, being around 40 degrees at low V/V_p, and going down to around 20 degrees at $V/V_p \approx 1$. Both the magnitude and the direction of the initial bow and side-wave velocity vector are taken Gaussian distributed at a given condition. Variances are modeled using available experimental data and the ESDU description.

Particle diameter: the particle diameter is derived from the particle Weber number in a way analogously as done by Croft (1998) and Kolev (1993).

Atomization fraction: Not all the water behind the wave front will be atomized. Part of just moves sideways. Therefore an atomization fraction AF is introduced, being the ratio of water atomized by the wave front, relative to the total volume of water initially present in the same part of the pool through which that wave front passed. The local atomization fraction has been related empirically to the local Froude number and the local initial velocity magnitude.

2.2 Flow field velocity

Due to particle inertia, small local areas of strong flow accelerations in the flow field around the aircraft (e.g. close to the stagnation line) have only little effect on the spray, as long as particles are larger than $O(0.1$ mm) in diameter. Therefore, basically, a uniform field with velocity equal to the airplane velocity is assumed. The advantage is that no extensive CFD calculations on the flow around the aircraft

have to be performed. However, if the regions with air-velocities differing from the undisturbed velocity become larger, this does no longer hold. Also the larger, more inert particles will have time to respond in that case. There are two corrections made to the uniform velocity field: the global, wing-induced velocity field and the entrainment velocities generated by the spray.

A large part of the spray passes under the wing. For a low-winged aircraft the mirror-effect of the ground increases the velocity field disturbance below the wing. For the Citation e.g. the ground surface is at around 1/3rd of the wing chord below the wing. This will lead to an extended region with low-speed air below the wing. Therefore, it was found necessary to model the circulation around the wing. As the interest is not in flow details close to the wing this is done in a simplified manner by putting a vortex-sheet at the wing chord and calculating the resulting flow field. The sheet, which stretches from 5 to 75 percent of the local wing chord *c*, has a constant distributed vortex strength such that the wing lift is represented correctly. The presence of the ground is taken into account by mirroring the vortex sheet with respect to the ground surface.

Thus far, no interaction between the droplets, constituting the spray, has been assumed. However, an indirect particle interaction that can not be neglected is the air entrainment velocity generated by the spray itself. This entrainment is caused by the drag forces acting on the separate droplets, which results in the air inside and close to the spray starting to move in the direction of the particles. This, in turn, reduces the relative velocity sensed by the particles and therefore lowers the drag forces on them. As a result the spray will rise higher. Because of the high density of the spray the entrainment effect is not insignificant. Therefore it is modeled by assuming that the air entrainment velocity is proportional to both the local particle density and the particle drag.

2.3 Aircraft modeling

In order to represent the aircraft body in the spray calculation, a number of elementary 'building blocks' has been defined in order to be able to quickly assemble an aircraft shape resembling the aircraft under study. Examples of the Cessna Citation II shape can be found in various figures in this report.

2.4 Spray results

Figure 2 shows results for a test case given in NASA TP 2718. A cross-ply tyre is used for this test, inflated to 35 psi. Aircraft speed is 60 ft/s, tyre load equals 500 lb and the pool depth equals 0.6 inch. The aircraft velocity, for the given tyre pressure, corresponds to almost 70% of the hydroplaning velocity. The parallelogram shaped ESDU envelope is also shown in figure 2.

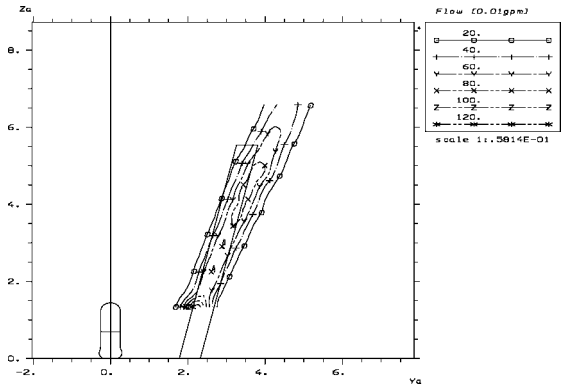

a) CR*spray calculation*

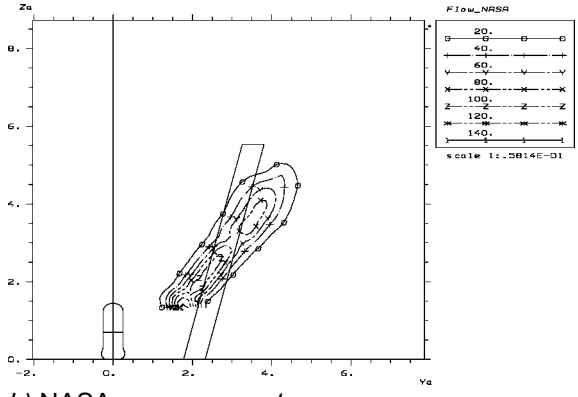

b) NASA *measurement*

Figure 2: NASA test case: spray density at 16.6 feet aft of tyre

Note that there is some discrepancy between the measured spray angle and the ESDU-envelope. Possibly, this is caused by the fact that the tyre is operated far below the rated pressure (55 psi) and therefore may have an uncharacteristic deformation. Nevertheless, it seems that a very reasonable comparison between CR*spray* calculation and measurement is obtained, especially as far as the vertical position and the level of spray density is concerned.

a. flight test

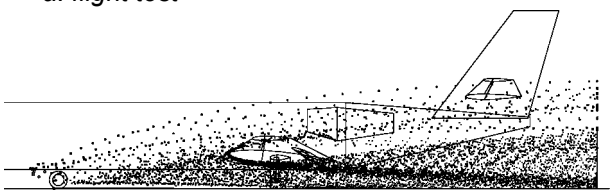

b. calculated nose gear spray

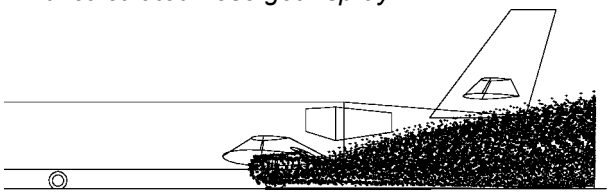

c. calculated main gear spray

Figure 3: Citation II: comparison of measured and calculated spray pattern at 80 kts.

A comparison between calculation and flight test for the Citation II is shown in figure 3. The main gear has a single 22x8 cross-ply tyre. The nose gear is equipped with a single, chined 18x4.4 cross-ply tyre. The main gear tyre pressure equals 9.6 bar (140 psi), the nose gear pressure equals 8.4 bar (120 psi) resulting in hydroplaning velocities equal to 106 and 99 kts respectively according to AMJ. Aircraft speed was 80 kts, about 70% of hydroplaning speed.

During the flight test hydroplaning started at speeds above 90 kts. Note that V_p is not equal to the actual velocity above which initial hydroplaning effects occur, but roughly equals the velocity were maximum tyre displacement drag occurs. For instance, data from Leland and Taylor (1966) show that tyre spin down starts from a velocity 8% below V_p.

The side views of the nose and main gear sprays (which are calculated separately) are shown in figure 3. Note that the main gear spray looks denser in the figure because it is a superposition of the left and right side spray of the port main gear, whereas only the left-hand side spray of the nose gear is shown. It is seen that the spray patterns agree excellently with the flight test results. Also the (partial) reflection of the nose spray on the wing is visible. The bow sprays are represented well.

Figure 4 shows the calculated impingement patterns. The upper half of each picture shows the impingement on the aircraft upper surface and the lower half the impingement on the lower surface. These data enable calculation of the impingement characteristics of the spray on the aircraft in terms of particle velocities and flow rates.

3 Calculation of precipitation drag

Precipitation drag consists of two main components, displacement drag and impingement drag. The first is a result of the work performed by the tyres breaking their way through the water pool. The second drag force is a result of the spray impinging on and flowing along the airframe. The displacement drag has been calculated using a slightly modified ESDU-method as given in ESDU 90035. The modification gives a better agreement between test data and model at velocities above hydroplaning.

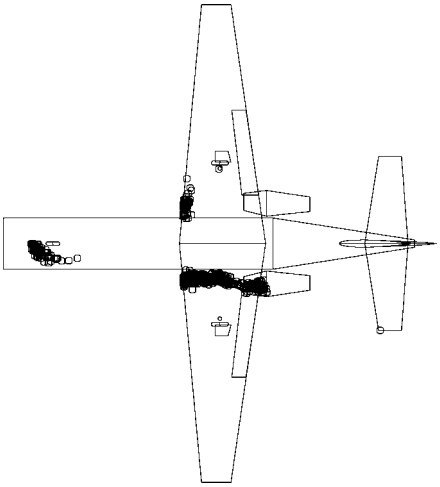

a) nose gear

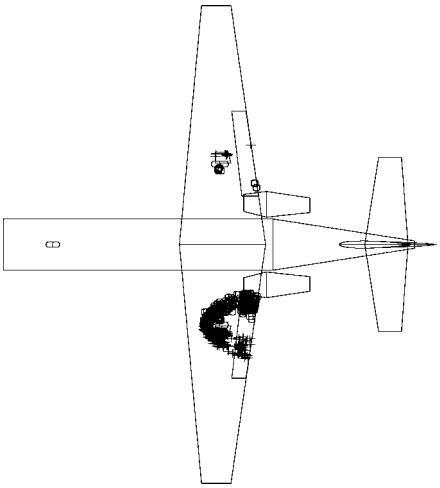

b) main gear

Figure 4: Citation II, 80 kts: calculated impingement pattern

To calculate impingement drag the spray is considered to consist of separate particles that hit the aircraft. Upon collision with the aircraft, the spray partly reflects off the surface. The remaining part adheres to the surface and forms a water film that flows over the aircraft surface. A partial elastic collision is assumed. The amount of reflection is given by the collision restitution coefficient *e*. The two main forces that contribute to the impingement drag are the collision force occurring at the moment of reflection and the surface shear force caused by the water boundary layer flow along the surface.

The collision force dominates at parts of the aircraft surface being normal to the direction of movement, like the wing leading edge. The water film (shear) drag force dominates at those parts of the surface being more or less parallel to the direction of movement. Although the contribution of the collision forces normally is larger, the water film shear force can not be neglected. Both drag contributions therefore have to be modelled. The method used for derivation of both forces is described hereafter. At present a very simple method giving good results is used. With increasing future knowledge the drag calculations can be further refined.

3.1 Collision force

Figure 5 shows the velocities of a particle before and after the partial elastic collision in the reflection plane. Normally, a spray droplet that hits the surface, results in a splash crater, with part of the incoming particle being absorbed by the water film and the rest being ejected again as a cloud of much smaller particles. For the present simple model the cloud may be represented by a single reflected particle, whereof the velocity is given by

$$\vec{G}_R = e(\vec{G}_P - 2\vec{G}_N) = e\{\vec{G}_P - 2(\vec{G}_P \bullet \vec{n})\vec{n}\}$$

Moreover, the incoming particle is assumed to impart a velocity G_F to the water film, equal to:

$$\vec{G}_F = (1-e)\vec{G}_T$$

where $\vec{G}_T$ is the surface tangential velocity component of the incoming particle. The water film velocity therefore is equal to zero for a fully elastic collision (e=1) and equal to the particle surface tangential velocity component for a fully inelastic collision (e=0).

The reflected and adhering particle mass flows are assumed to be related to the collision restitution coefficient as well:

$$\dot{m}_R = e\dot{m}_P$$

$$\dot{m}_F = (1-e)\dot{m}_P$$

The diameter of the reflected particle is reduced in accordance with the mass flow $\dot{m}_R$:

$$d_R^3 = \frac{\dot{m}_R}{\dot{m}_P} d_P^3$$

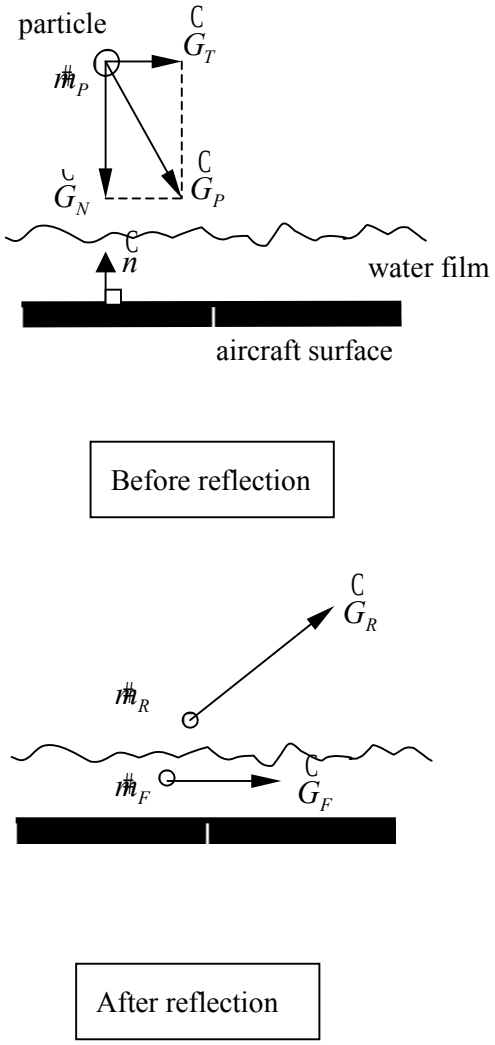

Figure 5: Partial elastic reflection of particle on aircraft surface

The collision force follows from the difference in the momentum vector before and after the collision:

$$\vec{F}_C = \dot{m}_P \vec{G}_P - \dot{m}_F \vec{G}_F - \dot{m}_R \vec{G}_R$$

So the drag-component of this collision force follows as:

$$D_C = \dot{m}_P \{U_P - eU_R - (1-e)U_F\}$$

(U is the component of the velocity in axial direction). A constant value for the restitution coefficient e is taken, although it is probable that e depends on various parameters, among which the droplet Weber number (describing the ratio of inertial and surface tension forces) and droplet incidence angle (Cossali, Coghe & Marengo, 1997). Unfortunately, little data is available on this subject. Haines and Luers (1983) postulate that the collision between (rain) droplets and the aircraft is fully inelastic. However, it has also been observed (Rockenbach & Alexander, 1980) that the ejected water volume was even *larger* than the incoming water volume under certain conditions (grazing angle, low droplet velocities) due to erosion of the water film by the impacting droplet. This would result in e being larger than 1. However, mostly part of the impinging droplet flow reflects, resulting in e being below one. Fortunately, the influence of e on the impingement drag is small due to the complementary drag effects of collision and surface shear drag. The value of the restitution coefficient e has been taken equal to 0.2.

3.2 Surface shear force

The surface shear force is determined from a boundary layer calculation. At present a simple approach is taken by considering this as a quasi-2D boundary layer flow and calculating the surface skin friction. A possible mutual effect of the sprays generated by different undercarriages is not taken into account. Also water film break up into rivulets is not taken into account. This happens at positions further downstream, where impingement rates get lower (Thompson and Marrochello, 1999).

The edge velocity of the water film boundary layer flow is taken equal to G_F. This assumption is valid as long as the density of the impacting water particles is large enough. At decreasing impact densities, e.g. further downstream the fuselage, the impact density may become so small that it is no longer capable of imposing the velocity at the edge of the water film. In the ultimate case of zero impact, the film edge velocity will be determined by the balance

between gravity forces, friction forces inside the film and the aerodynamic shear forces exerted by the flow on top of it. Due to the differences in viscosity between water and air, this will result in the film edge velocities going to relatively low values (this is illustrated e.g. by the long time it takes for the water film to clear the aircraft, after it has passed the water pool). In that case the film drag forces approach a value coined *absorption drag*. The absorption drag is the drag that follows from the assumption that those particles not being reflected are being absorbed by the surface, i.e. take on the aircraft velocity. This is the theoretical maximum of the surface shear drag. The absorption drag is independent of the location where the particle is obtaining the aircraft velocity. So, if the water film reaches the 'absorption condition' somewhere downstream, it is not necessary to calculate the film boundary layer development, but the absorption drag value can be used directly for that spray part. For the time being, the method always assumes that the water film edge velocities are dictated by the impacting droplets, resulting in the boundary layer development as described hereafter. Nevertheless, the theoretical maximum given by the absorption drag is checked for. If, for a given aircraft component, the shear drag exceeds the absorption drag, it is corrected.

Finally, a turbulent water film boundary layer is assumed, based on the results of McBride (1956). As it is not unlikely, however, that the water film flow will be laminar instead of turbulent in some cases, especially for lower film velocities, the turbulent boundary layer calculation is adapted by limiting the surface skin friction for conditions for which a partially laminar film flow may exist.

The local shear force is given by

$$\vec{\tau} = c_f \cdot \frac{1}{2}\rho \left|\vec{G}_F\right| \vec{G}_F$$

So, the local contribution to the impingement drag follows from

$$\Delta D_S = c_f \frac{1}{2}\rho \left|\vec{G}_F\right| U_F B_F \Delta X_A$$

B_F being the effective local impingement width (normal to X_a) and ΔX_A the step width in X-direction.

The boundary layer calculation is performed using the quadrature method of Bura (Schlichting, 1979), giving the development of the momentum loss thickness. Subsequently, the boundary layer and displacement thicknesses are estimated from the flat plate values:

$$\delta = \frac{72}{7}\theta \qquad \delta^* = \frac{\delta}{8}$$

The volume flow of water in this boundary layer per unit width then equals:

$$\int_0^\delta G dn = G_F(\delta - \delta^*) = 9 G_F \theta$$

This equation is used to determine the local effective impingement width B_F given the local, accumulated water film volume flow V_F and assuming the boundary layer thickness to be equal to the local water film thickness. So:

$$B_F = V_F / (9 G_F \theta)$$

Although a more precise method could be followed, by e.g. taking into account the actual impingement width, it was found that the method above gave the most consistent results.

In case of a fast lateral growth of the boundary layer, a correction is applied to the boundary layer run length to account for the relatively high shear contribution of those parts of the boundary layer with short run length and therefore relatively high skin friction.

4 Spray drag results

Results have been obtained for the three aircraft involved in the 'CONTAMRUNWAY'-project:

the Cessna Citation II, the Dassault Falcon 2000 and the SAAB 2000. Also results from a larger aircraft, the 100-seater Dassault Mercure, have been obtained. Further comparisons with large transport type aircraft data are still required to validate the method. The number of droplet trajectories calculated for each left/right side and centre spray equals 2500, although it is checked that the result is not sensitive to this number.

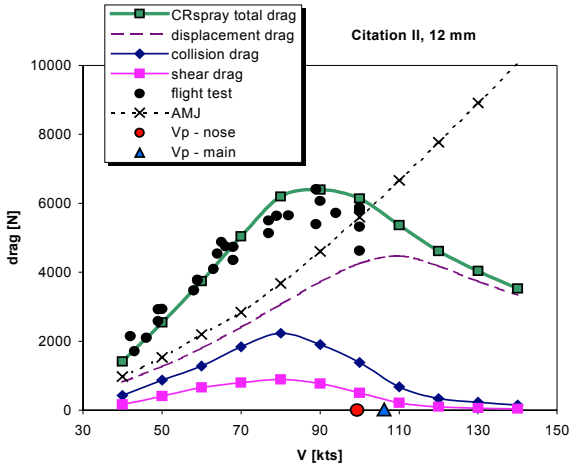

Figure 6: Citation II: CR*spray-results, compared with flight test data*

Figure 6 shows the precipitation drag for the Citation II for a pool depth of 12 mm. The CR*spray*-prediction is close to the measured data. The figure also shows the AMJ drag prediction, assumed valid for velocities below hydroplaning. It is seen to be significantly lower than the measurements. The total displacement drag of main and nose gear is also shown. Displacement drag is calculated according to the method given in ESDU 90035, except that at velocities above hydroplaning a $1/V^3$ decay has been taken, instead of the $1/V^2$ behaviour as taken by ESDU. This behaviour is believed to better represent the available experimental data as the latter would result in a constant displacement drag, which is not confirmed by the experimental data. Besides, ESDU 90035 (sketch 4.1) shows a displacement drag error bandwidth of around 40%, which is substantial. As it is difficult to obtain an accurate estimate of the frontal surface of the submerged part of the tyre, which depends not only on the *type* of tyre (radial or cross-ply) but possibly even on the *brand* of tyre, this error bandwidth does not surprise. It is believed that more research/better data is required in this area to obtain better displacement drag predictions.

The separate drag contributions (shear drag, collision drag and displacement drag) are shown as well. The nose gear is the main contributor to the collision drag. This collision drag is generated as the nose gear spray hits the wing leading edges. Although further experimental validation of the hypotheses underlying the drag calculation method is desired, it is not surprising that the almost normal impingement and retro-reflection of the spray in the airfoil nose region gives a large drag contribution.

Above hydroplaning the drag almost exclusively consists of displacement drag. The Citation is very pronounced in this respect due to the absence of a centre spray typical for side-by-side tyres. Such a centre spray, especially if generated by the nose gear, hits the fuselage not only at speeds below but also at speeds above hydroplaning, thereby causing a significant impingement drag at those speeds.

The influence of various parameters on the precipitation drag has been studied. Among those are: wing lift, pool depth, aircraft configuration (flap deflection) and the application of shined tyres. Some results for varying wing lift are shown here. For the Citation normally C_L = 0.4 is assumed during rolling. A calculation has been performed for zero lift as well. This affects both the tyre load, as well as the induced velocity field around the wing. Figure 7 shows the effects on drag.

Decreasing C_L results in a higher undercarriage load which, in turn, gives rise to a denser spray and increased impingement drag. If the flap is retracted (which will actually be the case if C_L has to be lowered) than the flap impingement drag contribution disappears, which reduces drag

again (drawn line). The net result is that the overall drag is roughly equal to the flap out drag at speeds below hydroplaning. This result is in line with the flight test that also showed small effects of flap settings below hydroplaning and a slight increase in drag above hydroplaning (open symbols).

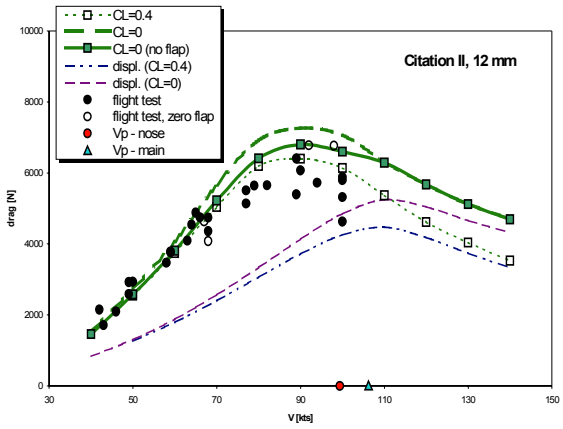

Figure 7: Citation II: effect of varying wing lift and flap deflection

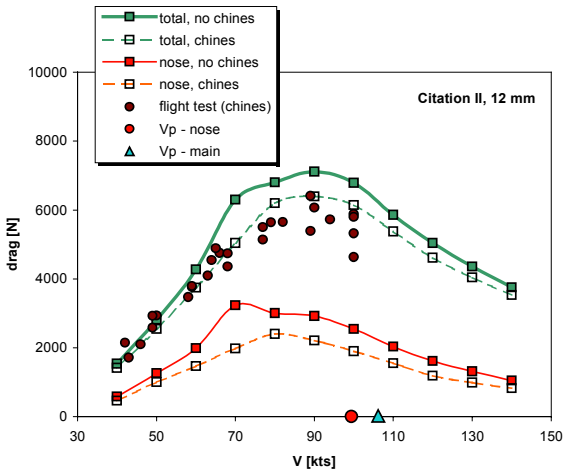

Figure 8: Citation II: influence of shines

Figure 8 shows the advantageous effect of the nose tyre shines. Shines are applied to reduce the risk of engine water ingestion. However, there is also an advantageous effect on precipitation drag as is clearly shown in this figure. This is due to a significant increase in nose spray impingement drag if no shines are applied. Engine ingestion follows as a natural side-result from CR*spray*. Without shines the maximum ingestion amounts to 0.015 m^3/s at 80 knots, which is considerable. With shines no ingestion occurs.

CR*spray* allows analysing the precipitation drag, e.g. by determining contributions of the various parts of the spray and the aircraft body. It is shown for instance that the bow wave spray gives a significant contribution to the precipitation drag. The main gear drag reduces to the displacement drag value without bow wave (figure 9). Often the effect of the bow wave is neglected, which is one of the main reasons for the discrepancy between flight test data and the AMJ-approach.

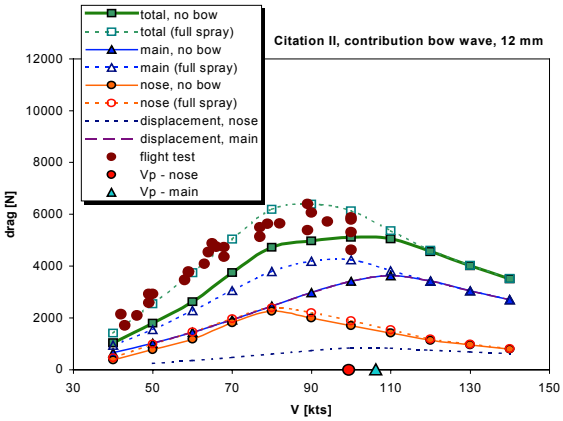

Figure 9: Citation II: contribution of bow wave to precipitation drag

Also the contribution of various parts of the airplane were studied separately. From this it appeared that parts of the undercarriage-structure as the struts and gear bay doors may give a significant contribution to the precipitation drag. A clear example of this was the gear doors of the SAAB 2000, located behind the tyres. These, relatively small, about 12" wide doors contributed to about 15 % of the impingement drag.

The influence of tyre pressure p_i is made visible in figure 10 for the Citation. The pressure of the main tyres is varied between +/- 10 percent. The sensitivity to hydroplaning reference velocity V_p is indicated in the figure (increasing velocity with increasing pressure). The effect on the

impingement drag is quite marked, with a decrease at higher speeds resulting from this shift in hydroplaning speed.

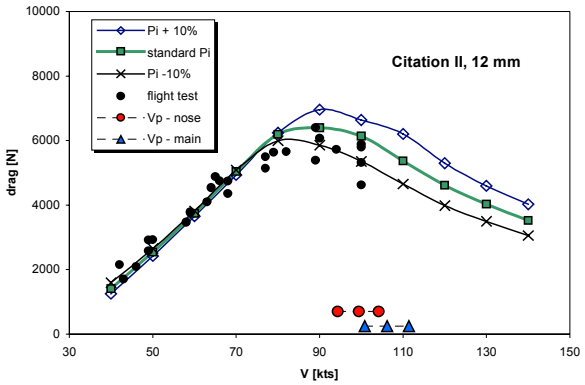

Figure 10: effect of tyre pressure Citation II

The AMJ-drag curves (not shown) are virtually independent of the tyre pressure. This sensitivity may explain the scatter in data-points around hydroplaning velocity, as it is difficult to keep tyre pressure constant during flight testing, due to heating of the tyres as a result of breaking at the end of each test run. Tyre pressure variations of 10% are common.

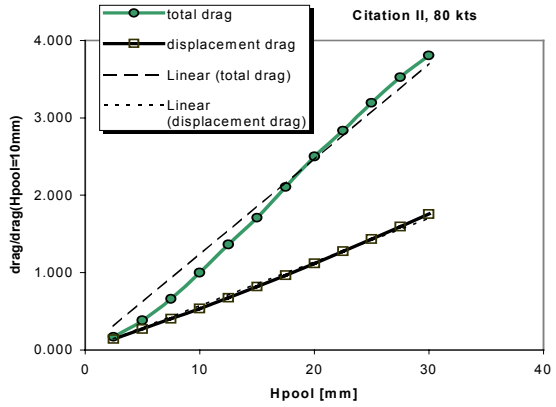

Figure 11: Citation II: non-linear precipitation drag development with poolheight

Often linear scaling is used to translate the results from one pool depth to another. Therefore it was interesting to have a closer look at this way of scaling. For this purpose the drag characteristics of the aircraft above have been calculated for different pool heights. The calculations were done for some velocities. Figure 11 shows the results at 80 knots. The curves show that it may not generally be assumed that the contamination drag is linear with pool depth. Non-linearity mainly comes from the nose-gear contribution. Linear scaling may be applied to some extent to the displacement drag curve.

5 Conclusions

A semi-empirical model has been developed to describe the sprays from aircraft undercarriages. Good agreement in spray shape with experimental data has been obtained.

The precipitation drag has been calculated on three smaller and one larger aircraft. The following conclusions can be drawn:

- Despite the fairly simple impingement drag model used, very acceptable overall precipitation drag results have been obtained;
- The method enables studying the effects of e.g. the bow wave, pool depth, flap settings and tyre pressures;
- The contribution of the bow wave to the impingement drag is significant;
- Linear scaling of precipitation drag with pool depth may not be considered a generally reliable method of scaling;
- More research is desired on the general validity of the displacement drag relation for modern tyres, especially at velocities around and above hydroplaning.
- It is advised to perform more validation of CR*spray* for larger aircraft.

6 References

BARRETT, R.B., "Drag and spray measurements from a pair of small pneumatic tyres placed side by side", Ministry of Aviation, S&T Memo 8/64, 1965.

BARRETT, R.B., "Drag and spray measurements from a small pneumatic tyre travelling through a water layer", Ministry of Aviation, S&T Memo 11/63, 1963.

COSSALI, G.E., COGHE, A., MARENGO, M.: "The impact of a single drop on a wetted solid surface", Experiments in Fluids, vol. 22, p.463-472, 1997.

CROFT N.: "Unstructured Mesh - Finite Volume Algorithms for Swirling, Turbulent, Reacting Flows", Thesis, University of Greenwich, London, 1998.

DAUGHERTY, R.H., STUBBS, S.M., "Measurements of flow rate and trajectory of aircraft tire-generated water spray", NASA TP 2718, 1987.

ESDU, "Estimation of spray patterns generated from the sides of aircraft tyres running in water or slush", ESDU 83042 with Amendment A, 1998.

ESDU: "Frictional and retarding forces on aircraft tyres. Part V: estimation of fluid drag forces", ESDU 90035, 1990.

GIESBERTS, M., "Precipitation drag measurements obtained in a pond for a Citation II", NLR TR 97574 L, 1997.

HAINES, P., LUERS, J.: "Aerodynamic penalties of heavy rain on landing airplanes", J. Aircraft, vol.20, no.2, 1983.

KOLEV N. I.: "Fragmentation and Coalescence Dynamics in Multiphase Flows", Experimental Thermal and Fluid Science, 6, 211-251 (1993).

LELAND, T.J.W., TAYLOR, G.R.: "An investigation of the influence of aircraft tire-tread war on wet-runway braking", NASA TN D-2770, 1966.

MALTBY, R.L., SLATTER, N.V.: "The measurement of the effects of slush and water on aircraft during take-off, part II: results of measurements on three aircraft", R&M 3604, 1969.

MCBRIDE, E.: "An experimental investigation of the scale relations for the impinging water spray generated by a planing surface", NACA TN 3615, 1956.

SCHLICHTING H.: "Boundary Layer Theory", McGraw Hill, 7th edition, 1979

THOMPSON, B.E., MARROCHELLO, M.R.: "Rivulet formation in surface-water flow on an airfoil in rain", AIAA Journal, vol. 37, no.1, 1999.